Scientific Research Publishing

International Journal of Clean Coal and Energy, 2026, 12(1), 1-30
https://www.scirp.org/journal/ijcce
ISSN Online: 2168-1538
ISSN Print: 2168-152X

Design and Airflow Distribution Characteristics of a Louver-Type Pulverized Coal Distributor Integrated into a Swirl-Straight Flow Synergistic Combustion Stabilization System

Longzhen Guo[1], Zhidong Li[2], Jiahui Zhao[3], Defu Xin[3], Weiyu Wang[4], Hanlin Li[4]*

[1]RunDian Energy Science and Technology Co., Ltd., Zhengzhou, China
[2]Hubei Chibi Electric Power Co., Ltd., Chibi, China
[3]Beijing Yelian Technology Co., Ltd., Beijing, China
[4]School of Energy Science and Engineering, Harbin Institute of Technology, Harbin, China
Email: *a1083698851@163.com

How to cite this paper: Guo, L.Z., Li, Z.D., Zhao, J.H., Xin, D.F., Wang, W.Y. and Li, H.L. (2026) Design and Airflow Distribution Characteristics of a Louver-Type Pulverized Coal Distributor Integrated into a Swirl-Straight Flow Synergistic Combustion Stabilization System. *International Journal of Clean Coal and Energy*, **12**, 1-30.
https://doi.org/10.4236/ijcce.2026.121001

Received: August 11, 2026
Accepted: September 25, 2026
Published: September 28, 2026

Abstract

With the increasing proportion of renewable energy generation, the demand for deep peak-shaving operation of coal-fired power units has been continuously intensified. Under low-load conditions, combustion stability issues caused by reduced pulverized coal feed, decreased furnace heat load, and lowered pulverized coal concentration have become increasingly prominent. Unlike conventional louver-type pulverized coal concentration separators, a pulverized coal distributor was coupled with a swirl-straight flow synergistic combustion stabilization system in this study. By regulating the air extraction ratio on the swirl side, the directional redistribution of the primary air-pulverized coal flow was achieved, thereby providing favorable aerodynamic conditions for the formation of a stable ignition zone under low-load operation. A combination of numerical simulation and cold-state experimental modeling was employed to investigate the internal flow characteristics, airflow distribution behavior, and pressure loss characteristics of the louver-type pulverized coal distributor. The results show that the louver blade structure can effectively alter the flow direction of the primary airflow, allowing a portion of the airflow to enter the swirl-side passage and achieving primary airflow redistribution. The inlet height of the swirl-side passage has a significant influence on the airflow distribution ratio, whereas the gradually expanding or contracting structures have a relatively limited effect on the pressure loss characteristics of the distributor. Considering the swirl-side airflow ratio, outlet velocity matching, and pressure loss characteristics comprehensively, when the swirl-side inlet height is set to 137 mm, the airflow entering the swirl side accounts for 15.17% of the total airflow, the velocity ratio between the two outlets is 1.03, and the overall pressure loss coefficient is 0.853. Although the pressure loss of this structure is slightly higher than that of some cases with lower inlet heights, it can satisfy the airflow supply requirement of the swirl side and achieve better outlet jet matching performance. Therefore, it is selected as the recommended structure. The results indicate that this structure can provide a reasonable primary airflow organization basis for the subsequent swirl-straight flow synergistic combustion system. However, the effects on pulverized coal concentration distribution and combustion stability improvement still require further verification through pulverized coal concentration measurements and combustion experiments. The numerical simulation results show good agreement with the experimental results. The simulated swirl-side airflow ratio is 15.28% of the total airflow, while the experimental value is 15.17%, corresponding to an absolute deviation of 0.11 percentage points and a relative error of 0.73%. These results indicate that the developed model can reasonably reproduce the selected integral airflow-distribution and pressure-loss characteristics of the distributor under the investigated cold-state single-phase conditions. The findings provide theoretical guidance and engineering references for the optimization of pulverized coal flow organization under deep peak-shaving conditions and for the retrofit of self-stabilizing combustion technologies in tangentially fired coal-fired boilers.

Keywords

Deep Peak-Shaving, Swirl-Straight Flow Synergistic Combustion Stabilization, Louver-Type Pulverized Coal Distributor, Airflow Distribution, Cold-State Modeling Experiment, Numerical Simulation

1. Introduction

With the large-scale development and utilization of renewable energy sources, such as wind and photovoltaic power, the uncertainty and intermittency of renewable energy generation in power systems have been continuously increased [1], thereby imposing higher requirements on the flexible regulation capability of conventional power sources [2]. As a crucial component of the power supply system in China, coal-fired power units continue to play an essential role in ensuring the secure and stable operation of the power grid and acilitating renewable energy integration [3] [4]. Therefore, improving the wide-load operating capability of existing coal-fired power units, particularly enhancing their stable operation capability under low-load conditions during deep peak-shaving operation, has become a key direction for the current flexibility-oriented retrofit of coal-fired power generation systems [5].

In response to the increasing demand for renewable energy accommodation, which has resulted in more frequent participation of coal-fired power units in peak-shaving operation, Wang *et al.* [5] proposed a multi-scale load regulation method based on the energy storage characteristics of steam turbines. By establishing a dynamic model of the power unit, the effects of different regulation strategies on load response capability were analyzed, and the rapid load regulation performance of the unit was improved. Furthermore, Wang *et al.* [6] developed an evaluation framework for the flexibility retrofit of coal-fired power units, in which the effects of boilers, steam turbines, auxiliary equipment, and other relevant components were comprehensively considered. This framework provided a decision-making basis for the implementation of customized flexibility retrofits for individual coal-fired power plants. Richter *et al.* [7] and Fiebrandt *et al.* [8] investigated feasible approaches for enhancing the flexibility of coal-fired power plants from the perspectives of operational characteristics and energy storage technology applications. It was indicated that reducing the minimum stable operating load and improving rapid load regulation capability are critical measures for enabling coal-fired power units to accommodate the increasing penetration of renewable energy.

Conventional coal-fired boilers are generally designed and optimized based on rated-load or high-load operating conditions. However, under low-load operation, the reduction in fuel input leads to a decrease in the concentration of the primary air-pulverized coal flow. Meanwhile, the reduction in the average furnace temperature decreases the radiative and convective heat transfer received by pulverized coal particles, thereby inhibiting volatile matter release, prolonging ignition delay, and reducing the combustion reaction rate. Consequently, flame stability deteriorates and combustion efficiency is decreased. For tangentially fired coal-fired boilers, the in-furnace combustion stability is primarily maintained by the swirling flow field generated by burner jets at each corner and the high-temperature flame heat transfer between adjacent burners. Under normal load conditions, the high-temperature flame formed by upstream adjacent burners can continuously provide ignition heat for downstream pulverized coal streams, thereby sustaining a stable combustion process. However, under deep peak-shaving conditions, the reduced pulverized coal supply and decreased furnace heat load significantly weaken the intensity of adjacent corner flames. As a result, sufficient ignition heat cannot be continuously supplied, and the ignition process of the pulverized coal flow is consequently restricted, ultimately reducing the minimum stable operating load of the boiler. Therefore, enhancing the ignition process of pulverized coal streams and improving flame stability under low-load conditions represent critical challenges that must be addressed for the deep peak-shaving operation of tangentially fired coal-fired boilers.

To address the deterioration of combustion stability under low-load conditions, extensive investigations have been conducted by researchers worldwide, mainly focusing on burner structure optimization, in-furnace aerodynamic field regulation, and enhancement of pulverized coal flow organization. Among these approaches, optimizing burner configurations and strengthening high-temperature recirculation zones have been recognized as effective strategies for improving low-load combustion stability. Wang *et al.* [9] proposed a novel swirl burner with an eccentric secondary air arrangement (NSB) to overcome the ignition difficulty of anthracite in down-fired boilers under deep peak-shaving conditions. The flow and combustion characteristics of the proposed burner were investigated through a combination of cold-state modeling experiments and industrial boiler operation tests. The results demonstrated that the proposed burner could enhance the intensity of the recirculation zone beneath the arch, improve the uniformity of pulverized coal concentration distribution, and increase the downward penetration depth of the airflow, thereby promoting more sufficient heat absorption by pulverized coal particles from high-temperature regions. Industrial test results indicated that the adoption of this burner reduced the minimum stable combustion load of the boiler from 150 MW to 90 MW, significantly enhancing the deep peak-shaving capability of the power unit. Chang *et al.* [10] employed a computational fluid dynamics (CFD) method to investigate the effects of burner tilt angles and arrangement configurations on the in-furnace flow field, temperature distribution, and NO_X emission characteristics of a 630 MW tangentially fired boiler operating under low-load conditions. It was found that optimized jet flow organization could improve the temperature distribution inside the furnace and enhance flame stability during low-load operation. Furthermore, Ma *et al.* [11] compared the combustion characteristics of tangentially fired boilers, opposed-firing swirl boilers, and down-fired boilers under low-load conditions. It was indicated that an appropriate reduction in operating oxygen concentration could promote the formation of localized reducing atmospheres, thereby improving combustion stability while suppressing NO_X formation. Overall, previous studies have demonstrated that the optimization of burner structures and regulation of in-furnace airflow organization can effectively improve flow field distribution and flame stability under low-load conditions. However, these approaches mainly rely on modifications to burner configurations or operating parameters, and their capability to directly enhance the intrinsic ignition characteristics of pulverized coal remains relatively limited.

In addition to burner structure optimization and in-furnace aerodynamic field regulation, enhancing the inherent ignition characteristics of pulverized coal has also been recognized as an important approach for improving combustion stability under low-load conditions. In recent years, various strategies, including pulverized coal preheating, pre-gasification, and combustion process decoupling, have been developed to increase the initial reactivity of pulverized coal and improve the ignition process under low-load operation. Tang *et al.* [12] proposed a novel low-NO_X burner equipped with a pulverized coal preheating function and investigated the effects of preheating temperature, air distribution mode, and load variation on the combustion process using a 40 MW pulverized coal-fired boiler test platform. The results indicated that pulverized coal preheating could increase the initial temperature of coal particles, promote volatile matter release, and shorten the ignition distance, thereby improving combustion stability under low-load operating conditions. Zhang *et al.* [13] developed a novel burner based on pre-gasification combustion technology, and its combustion performance was evaluated through a combination of CFD simulations and a 5 MW experimental platform. The results demonstrated that this technology could enhance the ignition process of pulverized coal under low-load conditions, enabling stable combustion to be maintained over a wider low-load operating range. To address the challenges associated with ignition difficulties and NO_X emission control during wide-load operation of low-volatile coal, Wang *et al.* [14] proposed a decoupled combustion technology. By separating the coal pyrolysis and char combustion processes, the residence time of pulverized coal particles in high-temperature regions was prolonged, thereby improving low-load combustion stability while simultaneously reducing NO_X formation. The aforementioned studies have demonstrated that improving the thermophysical properties of pulverized coal and enhancing the ignition reaction process can effectively improve the adaptability of boilers under low-load operation. However, technologies such as pulverized coal preheating and pre-gasification generally require additional energy input or complex auxiliary systems, which may result in challenges related to equipment investment and operational economy during engineering implementation. Therefore, utilizing the inherent transport characteristics of pulverized coal and achieving passive concentration enhancement through optimized pulverized coal flow organization have emerged as promising directions for the development of low-load combustion stabilization technologies.

In recent years, extensive studies have been further conducted on burner structure optimization and operating parameter regulation to address the challenge of ultra-low-load stable combustion during deep peak-shaving operation of coal-fired boilers. Previous investigations have demonstrated that the ignition and combustion stability under low-load conditions can be effectively improved by optimizing the matching relationship between primary and secondary air, enhancing localized recirculation zones, and regulating pulverized coal flow organization. Huang *et al.* [15] investigated the effects of central air on the flow field characteristics and low-load stability of a swirl burner through cold-state experiments and industrial tests conducted on a 700 MW boiler. It was found that reducing the central air flow rate could promote the earlier mixing of primary and secondary air streams, thereby improving flame stability. Ding *et al.* [16] proposed a novel internally circulating fluidized bed preheating combustion device equipped with an internal separator to address the ignition difficulty of low-volatile fuels. The gas-solid flow characteristics of the proposed system were analyzed through a combination of experimental and numerical approaches. Zhou *et al.* [17] investigated the effects of a pulverized coal concentrator, flame stabilization ring, and baffle structures inside a low-NOX swirl burner on the formation of ignition regions. The results indicated that appropriate pulverized coal concentration structures and recirculation organization could promote the formation of high-temperature and high-concentration regions, thereby enhancing combustion stability.

Furthermore, Liu *et al.* [18], Yang *et al.* [19], and Jiang *et al.* [20] investigated large-scale tangentially fired boilers under various load conditions. The results demonstrated that optimizing burner operation strategies and the primary-to-secondary air ratio could improve furnace temperature distribution and enhance operational stability under low-load conditions. Ju *et al.* [21] further indicated that coal properties exerted significant effects on the in-furnace temperature field, reducing atmosphere, and NO_x formation under low-load operation, and that appropriate coal selection and matching could improve overall combustion performance. Kim *et al.* [22] reported that the optimization of swirl structures could strengthen the formation of the central recirculation zone and prolong the residence time of pulverized coal particles in high-temperature regions, thereby facilitating coal ignition.

Overall, existing studies have mainly improved low-load combustion performance through burner structure optimization and operating parameter regulation. The underlying mechanisms primarily involve strengthening high-temperature recirculation, enhancing the mixing between pulverized coal and high-temperature flue gas, and improving local ignition conditions. However, these approaches mainly rely on regulation of the in-furnace flow field, while further optimization of the active control of primary air-pulverized coal concentration distribution remains necessary.

In summary, current low-load combustion stabilization technologies for coal-fired boilers mainly include operating parameter optimization, burner structure modification, and auxiliary combustion stabilization technologies. Operating parameter optimization can improve furnace flow characteristics and combustion conditions to some extent; however, its regulation range is restricted by boiler configurations and fuel properties. Auxiliary stabilization technologies, such as micro-oil ignition and plasma-assisted combustion, can provide additional ignition energy and improve combustion stability under low-load conditions, but they generally suffer from relatively high equipment investment costs and poor operational economy.

In contrast, autonomous combustion stabilization technologies that utilize the inherent characteristics of pulverized coal to enhance the ignition process without continuous auxiliary fuel input have gradually become an important development direction for deep peak-shaving retrofits of coal-fired boilers. Cao *et al.* [23] reviewed low-load combustion stabilization technologies for pulverized coal-fired boilers and indicated that increasing pulverized coal concentration, enhancing recirculation heat transfer, and improving gas-solid mixing processes are effective approaches for enhancing low-load combustion stability. Zhu *et al.* [24] applied preheating combustion technology to a tangentially fired boiler and achieved stable operation over a load range of 19% - 100%. Huang *et al.* [25] realized stable combustion of a low-quality coal-fired boiler at 30% load by optimizing central coal feeding, swirling slit air, and premixing structures.

Pulverized coal concentration separation technology is considered one of the effective approaches for improving pulverized coal combustion stability under low-load conditions. By separating the gas-solid two-phase flow in the primary air-pulverized coal stream, a coal-rich flow region can be generated locally, resulting in an increased pulverized coal concentration. This enhanced concentration promotes inter-particle heat transfer and radiative heat exchange, thereby facilitating volatile matter release and coal ignition, and ultimately improving combustion stability during low-load operation. Among various concentration separation devices, the louver-type pulverized coal concentrator, as a key component of horizontal rich-lean combustion technology, has been widely applied in large-scale pulverized coal-fired boiler combustion systems due to its simple structure, high separation efficiency, and relatively low pressure loss. Existing studies have mainly focused on the effects of louver structural parameters on pulverized coal separation performance, concentration enhancement, pressure loss characteristics, and internal gas-solid two-phase flow behavior. However, investigations into the coupled application of louver-type pulverized coal concentrators with low-load combustion stabilization systems in tangentially fired boilers remain relatively limited. In particular, the mechanisms associated with the formation of coal-rich regions through pulverized coal concentration separation and their influence on the combustion stability of swirl-straight flow synergistic combustion systems have not been sufficiently investigated. Nevertheless, previous studies on louver-type pulverized coal concentration technology have mainly concentrated on the enhancement of pulverized coal concentration, separation efficiency, and pressure loss characteristics. The flow redistribution mechanism when louver structures are employed as pulverized coal distribution units in low-load combustion stabilization systems, the optimization of the swirl-side air extraction ratio, and the matching relationship between the distributor and the combustion system remain insufficiently understood.

To address these issues, a swirl-straight flow synergistic combustion stabilization system based on a louver-type pulverized coal distributor is proposed in this study. The proposed system employs an externally installed louver-type pulverized coal distributor to achieve concentration separation and flow redistribution of the primary air-pulverized coal mixture. By regulating the distribution ratio of the primary air flow, a higher proportion of primary air-pulverized coal flow can be directed toward the swirl side, thereby providing favorable pulverized coal transport and combustion organization conditions for the subsequent swirl combustion region and improving the airflow matching characteristics within the swirl-straight flow synergistic combustion stabilization system.

A combination of cold-state modeling experiments and numerical simulations was adopted to investigate the internal flow characteristics, airflow distribution behavior, and pressure loss characteristics of the louver-type pulverized coal distributor. The effects of swirl-side inlet structural parameters on distributor performance were analyzed, and optimized structural parameters suitable for the swirl-straight flow synergistic combustion stabilization system were obtained. The results provide theoretical guidance and engineering references for optimizing primary air-pulverized coal flow organization and implementing autonomous combustion stabilization technologies in tangentially fired coal-fired boilers under deep peak-shaving conditions.

2. Model

2.1. Design Parameters

The research object investigated in this study is a 300 MW-class tangentially fired coal-fired boiler, with the model number of SG-1025/17.5-M4006. The boiler adopts a subcritical, single intermediate reheat, natural circulation, single-furnace, balanced-draft, and dry bottom ash discharge configuration. A low-NO_X concentric firing system is employed, in which burners are arranged at four corners with tangential firing technology. Tilting burners are additionally equipped to regulate the in-furnace aerodynamic field. The pulverizing system adopts a medium-speed mill positive-pressure direct-firing configuration, equipped with five coal mills, one of which serves as a standby unit. The coal mill model is ZGM95N-I medium-speed mill, coupled with CS2024HP electronic gravimetric belt feeders. The furnace cross-sectional dimensions are 12.800 m × 11.890 m, and the furnace height is 51.422 m. The original boiler combustion system consists of five layers of primary air nozzles, six layers of secondary air nozzles, one layer of compact over-fire air nozzles, and three layers of separated over-fire air nozzles. Based on the characteristics of the primary air-pulverized coal transport system of the investigated boiler, a swirl-straight flow synergistic combustion stabilization system was designed in this study, and the flow characteristics of the louver-type pulverized coal distributor incorporated in the system were investigated. The main design parameters of the boiler are listed in **Table 1**, and the fuel properties are summarized in **Table 2**.

Table 1. Main design parameters of the boiler.

Parameters	Symbol	Unit	Value
Superheated steam flow rate	D_{gr}	kg/s	265.27
Superheater outlet steam pressure	P''_{gr}	MPa	16.75
Superheater outlet steam temperature	T''_{gr}	˚C	535.03
Superheater outlet steam enthalpy	T''_{gr}	kJ/kg	3389.5
Reheater outlet steam flow rate	D_{zr}	kg/s	265.57
Reheater outlet steam pressure	P''_{zr}	MPa	3.28
Reheater outlet steam temperature	T''_{gr}	˚C	534.89
Reheater outlet steam enthalpy	H''_{gr}	kJ/kg	3532.9

Continued

Reheater inlet steam pressure	P'_{zr}	MPa	3.51
Reheater inlet steam temperature	T'_{zr}	˚C	328.41
Reheater inlet steam enthalpy	h'_{zr}	kJ/kg	3051.4
Economizer inlet feedwater temperature	T_{gs}	˚C	276.07
Economizer inlet feedwater pressure	P_{gs}	MPa	18.23
Economizer inlet feedwater enthalpy	H_{gs}	kJ/kg	1212.3
Effective heat utilization	Q	KJ	705417.78
Lower Heating Value efficiency	$\eta_{net,p}$	%	89.57
Input heat	Q_r	kJ/kg	16888

Table 2. Coal properties analysis.

Parameters	Value
Carbon (as received basis, %)	60.33
Hydrogen (as received basis, %)	3.62
Oxygen (as received basis, %)	9.94
Nitrogen (as received basis, %)	0.70
Total sulfur (as received basis, %)	0.41
Total moisture (%)	14.00
Ash (as received basis, %)	11.00
Volatile matter (dry ash-free basis, %)	36.50
Lower heating value (as received basis, MJ/kg)	22.76

2.2. Mathematical Model

To investigate the internal flow characteristics of the louver-type pulverized coal distributor, a computational fluid dynamics (CFD) method was employed to simulate the isothermal airflow behavior under cold-state conditions inside the distributor. Since this study primarily focuses on the velocity distribution, pressure variation, and flow redistribution characteristics of the primary air stream after passing through the louver structure, complex factors associated with pulverized coal particles were simplified. Accordingly, a single-phase incompressible air model was established. During the calculation process, the governing equations were discretized and solved using the finite volume method (FVM). The internal flow field distribution of the distributor was obtained through numerical simulations, and the reliability of the developed model was further validated by comparison with experimental results.

The flow inside the louver-type pulverized coal distributor represents a typical complex turbulent flow within a confined space. After entering the distributor, the primary air flow is redirected under the guidance of the louver blades. Meanwhile, due to the blockage effect of the blades and variations in flow passage cross-sectional area, complex flow phenomena, including velocity gradients, local pressure losses, and secondary flows, are generated inside the distributor. Therefore, an appropriate turbulence model is required to accurately describe the flow characteristics within the distributor.

Turbulence Model:

The fluid motion satisfies the conservation equations of mass, momentum, and energy. The governing equations are expressed as follows [26].

Continuity equation:

$$\frac{\partial \rho}{\partial t}+\frac{\partial}{\partial x_i}\left(\rho u_i\right)=0 \tag{1}$$

where u_i represents the mean velocity of the airflow in the i direction (m/s), and u_j represents the j direction component of the velocity vector.

Momentum equation:

$$\frac{\partial}{\partial t}\left(\rho u_i\right)+\frac{\partial}{\partial x_j}\left(\rho u_j u_i\right)=-\frac{\partial p}{\partial t}+\frac{\partial}{\partial x_j}\left[\mu\left(\frac{\partial u_i}{\partial x_j}+\frac{\partial u_j}{\partial x_i}\right)\right]+\sum \rho_s F_{si} \tag{2}$$

where x_j represents the j direction component of the velocity vector; u_j represents the mean velocity of the airflow in the j direction (m/s); p represents the pressure (Pa); μ represents the dynamic viscosity (kg/(m·s)); ρ_s represents the density of the fluid (kg/m^3); and F_{si} represents the external force component (N).

Energy equation:

$$\rho C_p \frac{\mathrm{d}T}{\mathrm{d}t}-\frac{\partial p}{\partial t}=\frac{\partial}{\partial x_j}\left(\lambda \frac{\partial T}{\partial x_j}\right)+\omega_s Q_s \tag{3}$$

where C_p represents the specific heat capacity of the fluid (J/(kg·K)); T represents the temperature (K); λ represents the thermal conductivity (W/(m·K)); ω_s represents the component reaction rate; and Q_s represents the component heat source (J).

The realizable k-ε model was selected as the turbulence model for the numerical simulations in this study [27]. Compared with the standard k-ε model, the realizable k-ε model exhibits superior prediction capability for complex flows involving swirl, jets, flow separation, and strong velocity gradients. It can more accurately capture the flow separation, secondary flow, and velocity redistribution induced by the louver blades. Therefore, the realizable k-ε model was employed to simulate the internal flow characteristics of the louver-type pulverized coal distributor. The corresponding transport equations are expressed as follows:

$$\frac{\partial(\rho k)}{\partial t}+\frac{\partial\left(\rho k u_i\right)}{\partial x_i}=\frac{\partial}{\partial x_i}\left[\left(\mu+\frac{\mu_t}{\sigma_k}\right)\frac{\partial k}{\partial x_j}\right]+G_k+G_b-\rho\varepsilon-Y_m+S_k \tag{4}$$

$$\frac{\partial(\rho\varepsilon)}{\partial_t}+\frac{\partial(\rho\varepsilon u_i)}{\partial x_i}=\frac{\partial}{\partial x_j}\left[\left(\mu+\frac{\mu_t}{\sigma_\varepsilon}\right)\frac{\partial\varepsilon}{\partial x_j}\right]+\rho C_{1\varepsilon}S_\varepsilon-\rho C_{2\varepsilon}\frac{\varepsilon^2}{k+\sqrt{v\varepsilon}}$$
$$+C_{1\varepsilon}\frac{\varepsilon}{k}G_b+S_\varepsilon \tag{5}$$

$$G_k=\mu_t\left(\frac{\partial u_i}{\partial x_j}+\frac{\partial u_j}{\partial x_i}\right)\frac{\partial u_i}{\partial x_i} \tag{6}$$

$$G_b=\beta g_i\frac{\mu_i}{Pr_t}\frac{\partial T}{\partial x_i} \tag{7}$$

where k represents the turbulent kinetic energy (m^2/s^2); ε represents the turbulent kinetic energy dissipation rate (m^2/s^3); μ_t represents the turbulent viscosity (Pa·s); σ_k and σ_ε represent the turbulent Prandtl numbers for the k and ε equations, respectively; G_k and G_b represent the generation terms of turbulent kinetic energy caused by mean velocity gradients and buoyancy effects, respectively; Y_m represents the contribution of fluctuating dilatation in compressible turbulence; S_k and S_ε represent user-defined source terms; $G_{1\varepsilon}$, $G_{2\varepsilon}$, $G_{3\varepsilon}$, and Pr_t represent empirical constants; β represents the thermal expansion coefficient; v represents the kinematic viscosity; and g_i represents the gravitational acceleration component in the i direction.

2.3. Evaluation Indicators

The parameters of the actual equipment and the scaled-down equipment are listed in Table 3.

Table 3. Parameters of the actual equipment and the scaled-down equipment.

Parameters	Symbol	Actual equipment	Scaled-down equipment
Geometric scale ratio	λ	1	0.5
Hydraulic diameter	D_h	0.546 m	0.273 m
Inlet area	A	0.234 m^2	0.0591 m^2
Average inlet velocity	U	22 m/s	22 m/s
Air density (20˚C)	ρ	1.205 kg/m^3	1.205 kg/m^3
Dynamic viscosity	μ	1.81×10^{-5} Pa·s	1.81×10^{-5} Pa·s

To evaluate the internal flow characteristics of the actual equipment and the scaled-down equipment, the Reynolds number is adopted as the criterion for flow similarity, and the calculation equation is given as follows [28]:

$$Re=\frac{\rho UD_h}{\mu} \tag{8}$$

where ρ represents the air density, kg/m^3; U represents the average inlet velocity of the distributor, m/s; D_h represents the hydraulic diameter, m; and μ represents the dynamic viscosity of air, Pa·s.

To ensure that the flow interaction between the swirl side and the lean side in the actual equipment and the scaled-down model remained consistent, the airflow momentum ratio is introduced [28]:

$$J = \frac{M_s}{M_l} \tag{9}$$

where M_s represents the airflow momentum on the swirl side, and M_l represents the airflow momentum on the lean side.

The airflow momentum flux was defined as follows:

$$M = \rho A U^2 \tag{10}$$

Scaled-down model momentum ratio [28]:

$$J = \frac{\rho_s A_s U_s^2}{\rho_l A_l U_l^2} \tag{11}$$

To verify the flow similarity between the actual equipment and the scaled-down model, further comparisons of the Reynolds number and momentum ratio under the two scales are performed. The Reynolds number is calculated using the inlet hydraulic diameter as the characteristic length. The results show that the Reynolds numbers of the actual equipment and the scaled-down model are 7.99×10^5 and 4×10^5, respectively. Both values are within the high-Reynolds-number flow regime ($Re > 10^5$), indicating that the requirements of the second self-modeling region are satisfied. Therefore, the scaled-down model is capable of reproducing the main flow characteristics of the actual equipment. Meanwhile, based on the airflow momentum calculation for the swirl side and lean side, the momentum ratios under the two scales are determined to be 0.185 and 0.185, respectively. The consistency of the momentum ratio demonstrates that the momentum distribution relationship between the two airflow streams in the actual equipment can be maintained in the scaled-down model. Therefore, the scaled-down model is considered suitable for cold-state experiments and numerical simulations (**Table 4**).

Table 4. Comparison of results between the actual equipment and the scaled-down equipment.

Parameters	Symbol	Actual equipment	Scaled-down equipment
Reynolds number	Re	7.99×10^5	4×10^5
Momentum ratio	J	0.185	0.185

The operating principle of the louver-type pulverized coal distributor is illustrated in **Figure 1**. After entering the distributor, the primary airflow is redirected by the louver blades and divided between two outlet passages. By adjusting the structural parameters of the distributor, the airflow fractions entering the two passages can be regulated to satisfy the air-distribution requirements of the downstream combustion system. Because only single-phase airflow was investigated in the present study, differences in pulverized coal concentration between the two outlets were not directly measured and therefore cannot be determined from the present results. According to the requirements of practical engineering applications, the outlets of the distributor are connected to the swirl burner and the straight-flow burner, respectively. The outlet passage connected to the swirl burner is defined as the swirl side, while the outlet passage connected to the straight-flow burner is defined as the straight-flow side. The swirl side is mainly used to supply the primary air-pulverized coal flow for the newly developed swirl burner, whereas the straight-flow side provides the primary air-pulverized coal flow for the original straight-flow burner. In the proposed system, the outlet connected to the swirl burner is intended to receive the coal-enriched stream expected from the conventional operating mechanism of a louver-type separator. This arrangement is designed to provide potentially favorable conditions for establishing a locally coal-rich region and improving ignition stability under low-load conditions. However, the pulverized coal concentration distribution and its influence on ignition stability were not measured in the present single-phase study and require verification through gas-solid two-phase and combustion experiments. Meanwhile, the lean pulverized coal flow is transported to the straight-flow burner to maintain the original straight-flow combustion mode. Therefore, in the following sections of this paper, the terms "swirl side" and "straight-flow side" refer to the outlet passages corresponding to different types of burners, whereas "rich side" and "lean side" represent the outlet passages classified according to pulverized coal concentration. These two definitions describe the outlet characteristics of the distributor from different perspectives, namely burner function and pulverized coal concentration distribution.

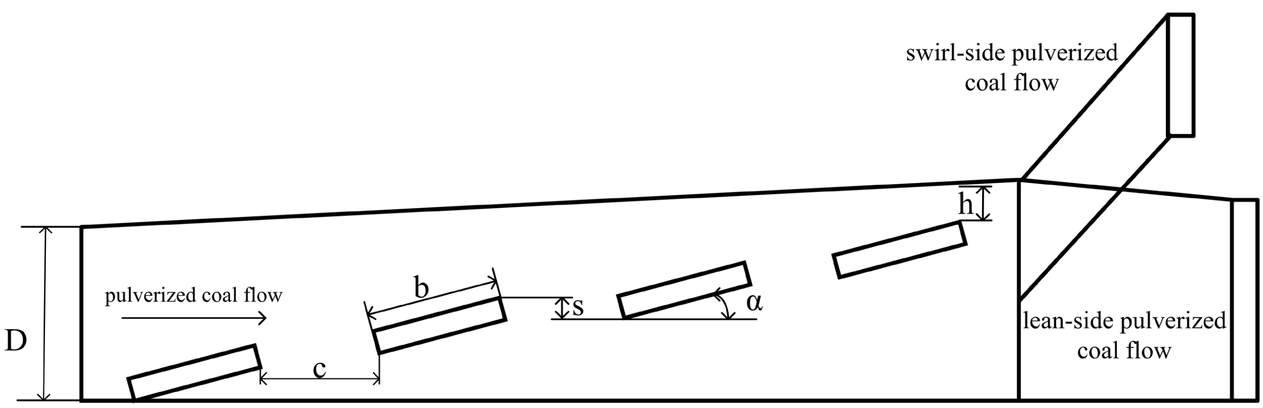

Figure 1. Schematic diagram of the louver-type pulverized coal distributor.

The louver-type pulverized coal distributor consists of a four-stage blade structure. The flow inside the distributor is approximately considered as a two-dimensional flow; therefore, the diffusion of airflow in the z direction is neglected in this study. The main structural parameters of the louver-type pulverized coal distributor include the distributor width D, blade width b, blade inclination angle α, blade spacing c, blade coverage height s, total blade blockage height h, number of blades n, and overall distributor length.

During the design process, the thickness of the distributor in the z direction is set as 0.759 m, and the width is defined as $D = 0.696$ m. The Reynolds number of the model is calculated to be approximately 1.85×10^5. Therefore, the airflow inside the distributor is located in the second self-similar region, indicating that the gas flow characteristics in the model can effectively represent the actual flow behavior inside the distributor.

The main dimensionless structural parameters of the concentrator are defined as follows [29]:

Blade spacing ratio:

$$d = \frac{x}{b \times \cos a} \tag{12}$$

Blade coverage ratio:

$$w = \frac{s}{b \times \sin a} \tag{13}$$

Blade blockage ratio:

$$z = \frac{h}{a} \tag{14}$$

The performance of the louver-type pulverized coal distributor is mainly evaluated based on the airflow velocity, pulverized coal flow rate, and pressure distribution at the inlet and outlets of the distributor. In this study, seven performance parameters are specifically defined.

Rich-to-lean air ratio:

$$R_Q = \frac{Q_n}{Q_d} \tag{15}$$

where Q_n represents the volumetric flow rate of the rich-side pulverized coal airflow (m^3/s); Q_d represents the volumetric flow rate of the lean-side pulverized coal airflow (m^3/s). The rich-to-lean air ratio is generally greater than 1 and is expected to approach 1, which ensures a more uniform velocity distribution of the rich and lean primary air streams at the burner outlet. More importantly, it contributes to achieving a higher concentration ratio of pulverized coal.

Rich-side airflow ratio:

$$\gamma_n = \frac{Q_n}{Q} \tag{16}$$

where Q represents the volumetric flow rate of the pulverized coal airflow at the concentrator inlet (m^3/s).

Lean-side airflow ratio:

$$\gamma_d = \frac{Q_d}{Q} \tag{17}$$

Total pressure loss coefficient:

$$\zeta = \frac{\Delta p_j}{\frac{\rho U_{in}^2}{2g}} \tag{18}$$

where Δp_j represents the static pressure difference between the inlet and outlet of the distributor (mmH_2O); $\frac{\rho U_{in}^2}{2g}$ represents the inlet dynamic pressure of the airflow (mmH_2O). A lower value of ζ is preferred, because an excessively high pressure loss coefficient can adversely affect primary air supply and pulverized coal transportation.

Rich-side pressure loss coefficient:

$$\zeta_n = \frac{\Delta p_n}{\frac{\rho U_{in}^2}{2g}} \tag{19}$$

where Δp_d represents the total pressure difference between the inlet and the rich-side outlet (mmH_2O), $\Delta P_d = \Delta P_j + \frac{\rho}{2g}\left(U_{in}^2 - U_d^2\right)$, and U_d represents the airflow velocity at the rich-side outlet (m/s).

Separation efficiency:

$$\eta = \frac{G_n}{G_o} \tag{20}$$

where G_n represents the pulverized coal mass flow rate on the rich side (kg/s), and G_o represents the pulverized coal mass flow rate at the concentrator inlet (kg/s).

In addition, certain relationships exist among the performance indicators of the louver-type pulverized coal distributor. These relationships can be used to facilitate the processing and analysis of experimental data:

$$R_c = \frac{1}{R_Q} \cdot \frac{1}{1/\eta - 1} \tag{21}$$

$$R_n = \eta \cdot \left(1 + \frac{1}{R_Q}\right) \tag{22}$$

$$R_n = \frac{R_c\left(R_Q + 1\right)}{R_c R_Q + 1} \tag{23}$$

3. Numerical Simulation and Experiments

Experimental Method

To investigate the internal airflow characteristics of the louver-type pulverized coal distributor and the effects of different structural parameters on airflow distribution, a cold-state single-phase experimental method is adopted. The experimental system mainly consists of an air supply system, an airflow measurement device, a louver-type pulverized coal distributor model, a pressure measurement device, and a data acquisition system.

A positive-pressure air supply mode is employed in the experiment. The inlet airflow velocity is controlled by adjusting the valve installed in the air supply pipeline. The total inlet airflow rate, outlet airflow rates on the swirl side and lean side, and system pressure loss are measured. To reduce the influence of random measurement errors, each operating condition is repeatedly tested three times, and the average value of the three measurements is taken as the final experimental result. During the experiment, the inlet airflow rate is maintained at a stable level to minimize the influence of airflow fluctuations on the measurement results. The overall configuration of the experimental setup and the louver-type pulverized coal distributor model are shown in **Figure 2**.

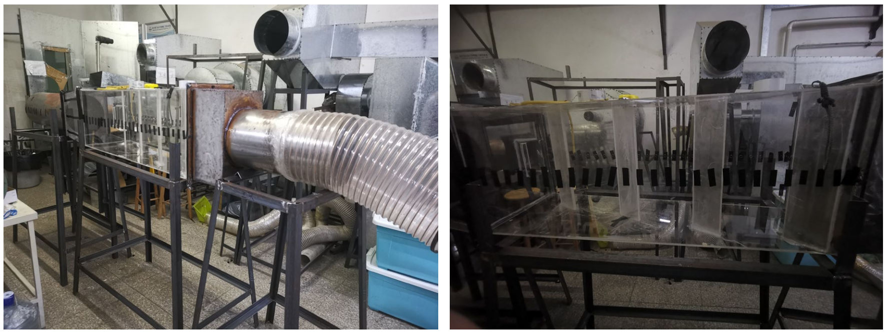

(a) (b)

Figure 2. Single-phase cold-state experimental test rig. (a) Photograph of the experimental test rig, (b) Photograph of the distributor model.

The airflow velocity is measured using an IFA300 constant-temperature hot-wire/hot-film anemometer manufactured by TSI, USA. The instrument provides a high temporal response and measurement accuracy, and therefore satisfies the requirements for measuring the outlet velocity distribution of the louver-type pulverized coal distributor. The measurement cross-sections at the swirl side and lean side outlets are arranged in the stable flow region downstream of the outlet. A multi-point sampling method is adopted for velocity measurement. During the measurement process, the probe is moved point by point along the outlet cross-section at equal intervals, ensuring that the measurement points cover the main flow region of the outlet. The local velocity at each measurement point is obtained, and the average velocity over the outlet cross-section is calculated based on the statistical analysis of multiple measurement results, thereby reducing the influence of local flow non-uniformity on the measurement accuracy. The hot-wire anemometry system and data acquisition device are shown in **Figure 3**.

To ensure that the flow conditions within the experimental model adequately represent the operating characteristics of the actual louver-type pulverized coal distributor, the cold-state modeling experiments are conducted according to the principles of geometric similarity, Reynolds-number similarity, and momentum-ratio similarity. The experimental model is scaled from the actual distributor at a geometric scale ratio of 1:2, while geometric similarity is maintained for all major structural parameters. According to similarity theory, when the Reynolds number $Re > 10^5$, the flow enters the second self-similar regime. Under this condition, the flow resistance and velocity distribution are governed primarily by the geometric

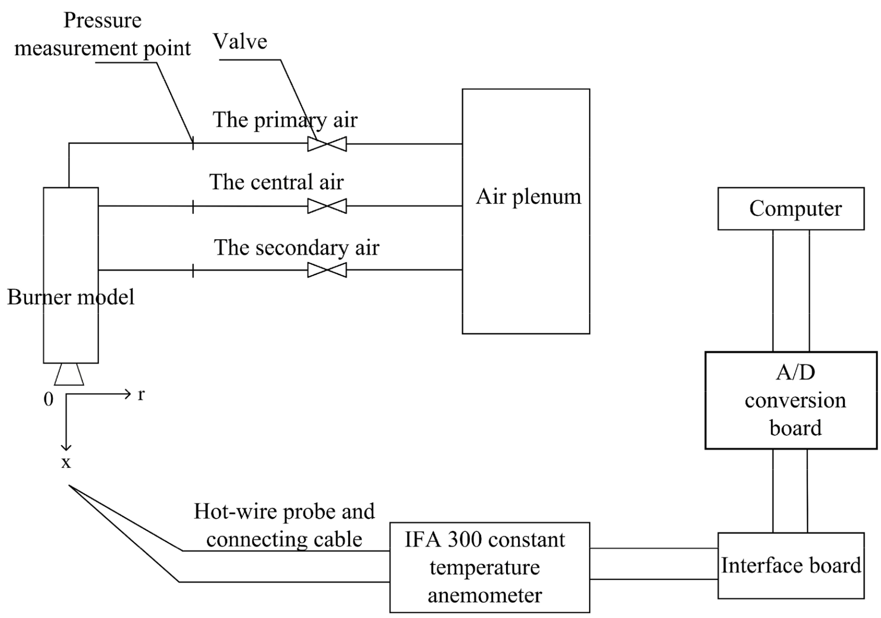

Figure 3. Hot-wire anemometry and data acquisition system.

configuration and are relatively insensitive to variations in the Reynolds number. In the present experiments, the Reynolds numbers of the airflow in the model ducts are all greater than 10^5, thereby satisfying the requirement for Reynolds-number similarity. In addition, according to the principle of momentum-ratio similarity, the inlet airflow rate of the model is adjusted so that the momentum ratios among the internal flow passages are consistent with those of the actual device. Consequently, satisfactory dynamic similarity is achieved between the experimental model and the actual louver-type pulverized coal distributor.

During the experiments, the total inlet airflow rate is measured using an averaging Pitot tube (Annubar-type flow probe) installed in the fully developed section of the air supply duct. The inlet airflow velocity is determined based on the cross-sectional average dynamic pressure obtained from the measurement section, and the total inlet airflow rate is calculated according to the cross-sectional area of the duct. Since the averaging Pitot tube is a non-standard flow measurement device, calibration is performed using a standard Pitot tube before the experiments. The measured cross-sectional flow rate obtained by the standard Pitot tube is used as the reference value to determine the calibration coefficient of the averaging Pitot tube, thereby reducing the systematic error in airflow measurement. The installation arrangement of the averaging Pitot tube is shown in **Figure 4**. The pressure loss across the louver-type pulverized coal distributor is measured using a static-pressure U-tube manometer. Because the outlets of the cold-state experimental system are exposed to ambient pressure, the liquid-column height difference measured by the U-tube manometer is used to determine the static pressure difference between the distributor inlet and outlets, thereby obtaining the system pressure loss. The outlet airflow rates on the swirl and lean sides are measured using Pitot tubes. The measurement sections are arranged in the stable flow regions downstream of the distributor outlets. The average dynamic pressure over each cross-section is obtained through multipoint measurements, and the mean airflow velocities and volumetric flow rates at the swirl-side and lean-side outlets are further calculated.

Figure 4. Schematic diagram of the arrangement of the Pitot tube in the air supply duct.

For the i-th measurement point obtained using the Pitot tube, the local velocity can be expressed as follows [30]:

$$U_i = \sqrt{\frac{2\Delta p_{d,i}}{\rho}} \tag{24}$$

where U_i represents the airflow velocity at the i-th measurement point, m/s; and $\Delta p_{d,i}$ represents the dynamic pressure at the i-th measurement point, Pa.

Based on the measurement results at each point, the cross-sectional average velocity $\bar{U}$ is obtained, and the outlet volumetric flow rate is calculated as follows:

$$Q = A\bar{U} \tag{25}$$

where A represents the effective flow area of the measurement cross-section, m^2; and $\bar{U}$ represents the cross-sectional average velocity, m/s.

To evaluate the uncertainty propagation of the experimental measurement error to the airflow rate and pressure loss coefficient, an uncertainty analysis is performed. Under the condition that the input quantities are mutually independent, the combined relative standard uncertainty of the air volumetric flow rate can be expressed as follows [31]:

$$u_r(Q) = \sqrt{\left[\frac{u(A)}{A}\right]^2 + \left[\frac{u(\bar{U})}{\bar{U}}\right]^2} \tag{26}$$

where $u(A)$ represents the standard uncertainty of the flow area; and $u(\bar{U})$ represents the standard uncertainty of the cross-sectional average velocity.

For the velocity measured by the Pitot tube, its relative standard uncertainty can be further expressed as follows:

$$u_r\left(\bar{U}\right)=\frac{1}{2}\sqrt{\left[\frac{u\left(\Delta p_d\right)}{\Delta p_d}\right]^2+\left[\frac{u\left(\rho\right)}{\rho}\right]^2} \tag{27}$$

where $u\left(\Delta p_d\right)$ represents the standard uncertainty of dynamic pressure measurement; and $u\left(\rho\right)$ represents the standard uncertainty of air density.

According to the first-order uncertainty propagation relationship and the definition equation of the pressure loss coefficient, the relative standard uncertainty is obtained as follows:

$$u_r\left(\zeta\right)=\sqrt{\left[\frac{u\left(\Delta p\right)}{\Delta p}\right]^2+\left[\frac{u\left(\rho\right)}{\rho}\right]^2+\left[2\frac{u\left(U_0\right)}{U_0}\right]^2} \tag{28}$$

where $u\left(\Delta p\right)$, $u\left(\rho\right)$, and $u\left(U_0\right)$ represent the standard uncertainties of pressure loss, air density, and inlet average velocity, respectively.

To investigate the influence of the swirl-side inlet geometry on the airflow distribution performance of the louver-type pulverized coal distributor, the main distributor structure is kept unchanged while different test conditions are established by varying the swirl-side inlet height. Six inlet heights are considered: 146 mm, 137 mm, 132 mm, 127 mm, 120 mm, and 116 mm. The corresponding structural configurations are shown in **Figure 5**.

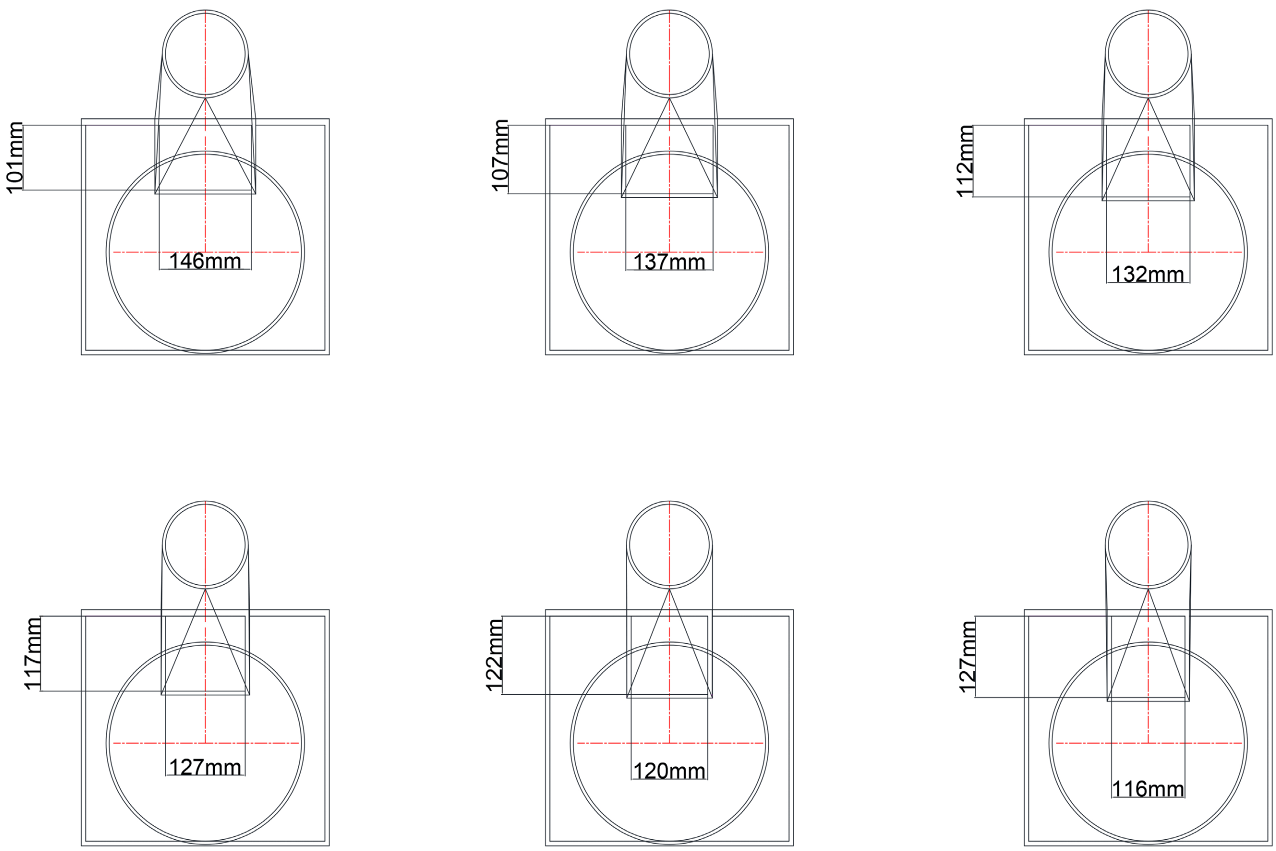

Figure 5. Configurations of the louver-type pulverized coal distributor with different swirl-side inlet heights (from left to right and from top to bottom: Cases 1 - 6).

Based on the cold-state experimental results, the operating condition with a swirl-side inlet height of 137 mm is selected for the numerical simulation. The computational model is established according to the dimensions of the experimental model, and the test section of the distributor is 2.672 m in length. To minimize the influence of the inlet and outlet boundary conditions on the internal flow field, a 1 m inlet development section and a 0.9 m outlet development section are added to the computational domain. The computational domain is discretized using a three-dimensional multi-block structured mesh composed of hexahedral cells. To ensure sufficient numerical accuracy, local mesh refinement is applied in the louver-blade region, the swirl-side inlet region, and regions where the flow-passage cross-section changes. Grid-independence analysis is performed using three meshes with coarse, medium, and fine resolutions, containing approximately 1.50 million, 2.55 million, and 4.00 million cells, respectively. The swirl-side outlet velocity and the overall pressure loss coefficient are selected as the evaluation parameters. The results show that increasing the mesh size from approximately 2.55 million to 4.00 million cells results in only minor variations in the key evaluation parameters, with the maximum deviation remaining below 2%. Therefore, the mesh containing approximately 2.55 million hexahedral cells is adopted for the subsequent calculations, providing an appropriate balance between computational accuracy and efficiency. The computational model and mesh configuration are shown in **Figure 6**.

Figure 6. Computational model and mesh configuration of the louver-type pulverized coal distributor.

The inlet boundary conditions for the numerical simulations are specified according to the cold-state experimental conditions. The inlet adopts a velocity-inlet boundary condition, with the average inlet velocity set to 22 m/s. The inlet turbulence parameters are defined using the turbulence intensity and hydraulic diameter, with the turbulence intensity set to 10%. The hydraulic diameter of the actual equipment is 0.546 m, while the hydraulic diameter of the cold-state experimental model and numerical simulation model is 0.273 m, which is established according to the geometric scale ratio of 1:2 between the model and the actual equipment. A pressure-outlet boundary condition is imposed at the outlet to represent fully developed pipe-flow conditions. All solid walls are treated as no-slip boundaries to account for the restriction imposed by the distributor walls on the airflow. During the numerical calculations, the governing equations are spatially discretized using the third-order MUSCL scheme to reduce numerical diffusion and improve spatial accuracy. Pressure-velocity coupling is achieved using the SIMPLE algorithm, while the PRESTO scheme is employed for pressure interpolation. Convergence is considered to be achieved when the residuals of all governing equations decrease below 10^{-4}.

4. Results and Discussion

4.1. Effect of Swirl-Side Inlet Height on Distribution Performance

The experimental results obtained for different swirl-side inlet configurations are presented in Table 5. The swirl-side inlet height is a key structural parameter governing the redistribution of the primary air-pulverized coal flow. Variations in this parameter not only alter the effective flow area at the swirl-side inlet, but also affect the local pressure distribution in the louver region and the extent of airflow deflection. Consequently, the swirl-side inlet height directly determines the proportion of airflow entering the swirl-side passage and the matching of jet momentum between the two outlets. As shown in Table 5, variations in the swirl-side inlet height lead to pronounced changes in the swirl-side outlet velocity, airflow distribution ratio, and system pressure loss. These results indicate that the inlet geometry exerts a significant influence on the internal flow organization of the distributor.

Table 5. Experimental results of the louver-type pulverized coal distributor.

Parameters	Unit	Case 1 146 mm 38.42%	Case 2 137 mm 36.05%	Case 3 132 mm 34.74%	Case 4 127 mm 33.42%	Case 5 120 mm 31.58%	Case 6 116 mm 30.53%
Swirl-side airflow velocity	m/s	14.16	15.56	14.19	15.0	12.85	12.6
Lean-side airflow velocity	m/s	15.56	15.08	15.25	15.5	15.68	15.9
Swirl-side/lean-side velocity ratio	-	0.91	1.03	0.93	0.97	0.82	0.79
Swirl-side airflow rate	m^3/h	646.03	709.46	647.53	684.15	603.69	574.18
Lean-side airflow rate	m^3/h	4093.57	3967.23	4010.54	4086.25	4125.29	4171.57
Swirl-side/lean-side airflow-rate ratio	%	15.75	17.88	16.14	16.74	14.63	13.76
Swirl-side airflow fraction of the total airflow	%	13.63	15.17	14.0	14.34	12.81	12.10
Design swirl-side airflow fraction	%	11.74	11.74	11.74	11.74	11.74	11.74
Experimental-to-design swirl-side airflow ratio	-	1.161	1.292	1.193	1.221	1.091	1.031
Pressure loss coefficient of the square-to-round transition on the swirl side	-	0.7288	0.3049	0.5161	0.4902	1.0	1.1195
Overall pressure loss coefficient with the swirl side open	-	0.908	0.853	0.817	1.078	0.895	0.602
Pressure loss coefficient with the swirl side closed	-	-	0.974	1.125	1.033	0.886	-

To satisfy the primary air flow organization requirements of the swirl-straight flow synergistic combustion stabilization system, the airflow distribution ratio on the swirl side, outlet velocity matching, and system pressure loss are selected as the main evaluation indicators for optimizing the inlet height of the swirl-side passage. According to the system design parameters, the designed airflow ratio on the swirl side accounts for 11.74% of the total airflow. The engineering design specified a nominal swirl-side airflow fraction of 11.74%, but no strict acceptance ranges are prescribed for the airflow fraction, outlet velocity ratio, or pressure loss coefficient. The nominal swirl-side airflow fraction of 11.74% is used as an engineering reference rather than as a strict set point, because no predetermined acceptance ranges are available for the airflow fraction, outlet velocity ratio, or pressure-loss coefficient. The outlet velocity ratio is treated as the primary comparative criterion, followed by the overall pressure-loss coefficient and the swirl-side airflow-supply capability. The 137 and 127 mm configurations produced velocity ratios of 1.03 and 0.97, respectively, and are therefore equally close to unity. However, the 137 mm configuration exhibited a lower overall pressure-loss coefficient than the 127 mm configuration (0.853 versus 1.078). Although the 132 mm configuration produced a slightly lower pressure-loss coefficient of 0.817, its outlet velocity ratio of 0.93 deviated further from unity. Therefore, among the six investigated configurations, the 137 mm configuration is selected as the preferred engineering compromise. This selection is comparative and should not be interpreted as a universal optimum. The selection of the preferred configuration represents a trade-off among these indicators rather than compliance with predetermined acceptance limits.

When the swirl-side inlet height decreases from 146 mm to 137 mm, the swirl-side outlet velocity increases from 14.16 m/s to 15.56 m/s, corresponding to an increase of approximately 9.9%. Meanwhile, the swirl-side airflow rate increases from 646.03 m^3/h to 709.46 m^3/h, and its proportion of the total airflow rises from 13.63% to 15.17%. This behavior is mainly attributed to the reduction in the effective inlet area on the swirl side. As the inlet height is moderately reduced, part of the airflow that originally travels along the main flow direction is more strongly constrained by the inlet boundary and is therefore more readily deflected laterally under the guidance of the louver blades. As a result, the transverse momentum directed toward the swirl-side passage is enhanced. In addition, a moderate reduction in inlet height strengthens the pressure gradient near the swirl-side inlet, further promoting lateral flow deflection and improving the air extraction capability of the swirl-side passage. Thus, as the inlet height decreases from 146 mm to 137 mm, the airflow redistribution capability of the distributor is progressively enhanced.

However, further reduction in the swirl-side inlet height does not lead to a continued increase in the extracted airflow. When the inlet height decreases from 137 mm to 116 mm, the swirl-side outlet velocity decreases from 15.56 m/s to 12.60 m/s, while the swirl-side fraction of the total airflow decreases from 15.17% to 12.10%. This decline is mainly associated with the intensified local contraction effect caused by an excessively small inlet. As the airflow passes through the narrowed region, larger velocity gradients and greater local pressure losses are generated, thereby reducing the effective flow rate through the swirl-side passage. Moreover, with a further decrease in inlet height, the restriction imposed by the flow passage becomes stronger and the local high-velocity region expands. A greater proportion of the available pressure difference is consequently dissipated in overcoming local flow resistance rather than being converted into an increase in swirl-side airflow.

Therefore, a transition exists from enhanced airflow deflection to increased flow blockage as the swirl-side inlet height is reduced. An excessively small inl*et al*so limits the effective area available for airflow entering the swirl-side passage, thereby weakening the redistribution effect induced by the louver structure. Accordingly, the relationship between the swirl-side inlet height and the air extraction capability is not simply monotonic; instead, an optimum matching range exists.

Therefore, a transition exists from enhanced airflow deflection to increased flow blockage as the swirl-side inlet height is reduced. An excessively small inl*et al*so limits the effective area available for airflow entering the swirl-side passage, thereby weakening the redistribution effect induced by the louver structure. Accordingly, the relationship between the swirl-side inlet height and the air extraction capability is not simply monotonic; instead, an optimum matching range exists.

Further analysis of the velocity matching between the swirl-side and lean-side outlets indicates that, when the swirl-side inlet height is 137 mm, the outlet velocity on the swirl side is 15.56 m/s, whereas that on the lean side is 15.08 m/s. The resulting velocity ratio reaches 1.03, which is close to the ideal condition. A high degree of velocity matching ensures a coordinated momentum distribution of the inlet airflow to the subsequent swirl burner and straight-flow burner, thereby avoiding deviations in the in-furnace aerodynamic field caused by excessive differences in jet velocity between the two sides. For tangentially fired boilers, the jet momentum distribution of the burners directly affects the stability of the rotating flow field in the furnace. If the outlet velocities on the swirl side and straight-flow side differ excessively, local jet penetration capability may be altered, and the in-furnace aerodynamic field may be shifted accordingly. Therefore, while the enhancement of pulverized coal concentration is required, a reasonable velocity matching relationship between the two outlet streams should also be ensured.

By contrast, when the inlet height is reduced to 116 mm, although the overall pressure loss coefficient of the system decreases to 0.602, the velocity ratio between the swirl side and the lean side is only 0.79. This indicates that the outlet velocity on the swirl side is substantially lower than that on the straight-flow side, resulting in unfavorable outlet velocity matching between the two passages. Therefore, when evaluating the performance of the louver-type pulverized coal distributor, pressure loss alone cannot be regarded as the sole criterion. The swirl-side airflow supply and outlet velocity ratio should also be considered. The airflow redistribution capability and outlet velocity matching should also be comprehensively considered. Among the six configurations, the 137 mm case provides the closest outlet velocity matching, with a swirl-side/straight-flow-side velocity ratio of 1.03. Its swirl-side airflow fraction of 15.17% exceeds the design value of 11.74%, while its overall pressure loss coefficient of 0.853 is not the lowest among the investigated cases. Therefore, the 137 mm configuration is selected primarily because it provides the best outlet velocity matching while maintaining sufficient swirl-side airflow supply and a moderate pressure loss. This selection represents a multi-criteria engineering trade-off rather than the optimization of any single indicator. Overall, the 137 mm configuration provides the most favorable compromise among outlet velocity matching, swirl-side airflow supply, and system pressure loss.

4.2. Analysis of the Internal Flow Characteristics of the Louver-Type Distributor

To further elucidate the influence of the louver structure on the flow behavior of the primary air-pulverized coal stream, numerical simulations are performed to analyze the internal velocity field of the distributor under the condition with a swirl-side inlet height of 137 mm. Figure 7 presents the velocity distribution on the central section of the louver-type pulverized coal distributor. The velocity distributions at the swirl-side and lean-side inlet sections are also shown in Figure 7.

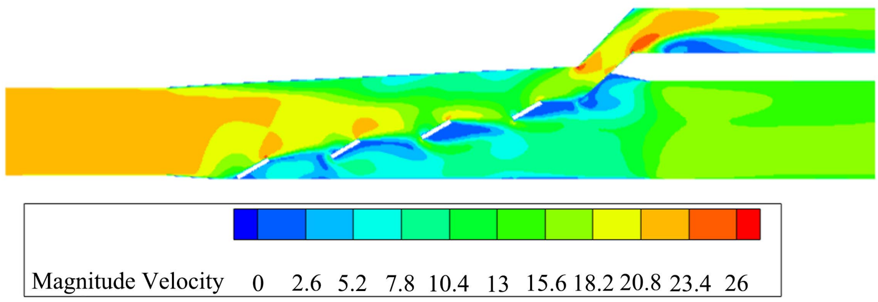

Figure 7. Velocity distribution on the central widthwise section of the louver-type pulverized coal distributor.

As shown in Figure 7 and Figure 8, the primary airflow undergoes pronounced deflection after entering the distributor under the guiding effect of the louver blades, resulting in the formation of two major flow regions. The airflow adjacent to the blades is redirected by the blade blockage and gradually enters the swirl-side passage, whereas the remaining airflow continues approximately along its original direction and ultimately enters the lean-side passage. Near the leading edges of the blades, the abrupt change in the flow-passage cross-section accelerates the airflow and produces local high-velocity regions. Meanwhile, flow separation occurs on the leeward sides of the blades, giving rise to low-velocity and locally negative-pressure regions. This non-uniform velocity distribution constitutes an important mechanism by which the louver structure induces airflow deflection and redistribution.

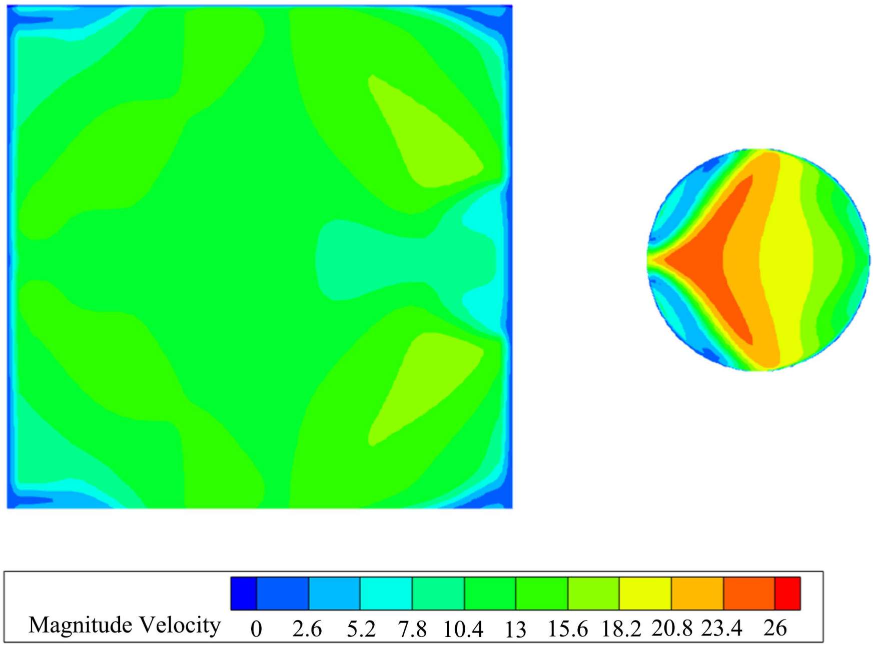

Figure 8. Velocity distributions at the swirl-side and lean-side inlet sections.

As the airflow proceeds toward the outlets, pronounced velocity gradients develop in the swirl-side passage because of the curved flow path and variations in the passage cross-section. Owing to the centrifugal effect in the bend, the airflow velocity on the outer side of the curved passage is higher than that on the inner side. After passing through the downstream development section, however, the velocity distribution gradually becomes more uniform. This indicates that the outlet development section plays an important role in improving airflow uniformity.

From the perspective of the overall flow process, the louver blades do not simply divide the airflow mechanically. Instead, the redistribution of the primary air flow is achieved by changing the local pressure distribution and flow direction. Therefore, the proportion of primary air flow entering the swirl side and lean side can be regulated through reasonable design of the inlet structural parameters, providing suitable airflow matching conditions for the subsequent swirl-straight flow synergistic combustion system. It should be noted that the single-phase air model and cold-state experimental method adopted in this study are mainly used to verify the influence of the louver structure on airflow distribution characteristics. The redistribution of pulverized coal concentration and its effects on the combustion process require further investigation through gas-solid two-phase experiments and combustion tests.

4.3. Comparison between Numerical Simulation and Experimental Results

To validate the reliability of the numerical model in predicting the flow characteristics of the distributor, the simulation results are compared with the cold-state experimental data, as presented in Table 6.

Table 6. Comparison between experimental and numerical results for the louver-type pulverized coal distributor.

Parameters	Experimental result	Numerical result	Absolute deviation	Relative error
Swirl-side outlet velocity	15.56 m/s	14.98 m/s	0.58	3.73%
Lean-side outlet velocity	15.08 m/s	14.01 m/s	1.07	7.10%
Swirl-side/lean-side velocity ratio	1.03	1.07	0.04	3.88%
Swirl-side airflow fraction of the total airflow	15.17%	15.28%	0.11	0.73%
Pressure loss coefficient of the square-to-round transition on the swirl side	0.30	0.32	0.02	6.67%
Overall pressure loss coefficient	0.853	0.87	0.017	1.99%

As shown in **Table 6**, the numerical simulation results are generally consistent with the experimental measurements in terms of the overall trends. To quantitatively evaluate the prediction accuracy of the numerical model, the relative errors of each evaluation parameter are further calculated. The relative error is defined as the absolute difference between the simulated and experimental values divided by the experimental value. The simulated and experimental swirl-side outlet velocities are 14.98 m/s and 15.56 m/s, respectively, with a relative error of 3.73%. The simulated and experimental lean-side outlet velocities are 14.01 m/s and 15.08 m/s, respectively, with a relative error of 7.10%. The simulated velocity ratio between the two outlets is 1.07, compared with the experimental value of 1.03, resulting in a relative error of 3.88%.

For airflow distribution, the simulated swirl-side airflow ratio is 15.28% of the total airflow, while the experimental value is 15.17%. The absolute deviation between the two values is only 0.11 percentage points, corresponding to a relative error of 0.73%. In terms of pressure loss characteristics, the simulated pressure loss coefficient of the swirl-side circular duct is 0.32, compared with the experimental value of 0.30, resulting in a relative error of 6.67%. The simulated overall pressure loss coefficient is 0.87, while the experimental value is 0.853, with a relative error of 1.99%. The differences between the numerical and experimental results can mainly be attributed to several factors. The numerical model neglects the two-phase coupling between pulverized coal particles and the airflow; small deviations in local flow-passage dimensions may also arise from manufacturing tolerances in the experimental model. In addition, measurement uncertainties are inevitably introduced during hot-wire velocity and pressure measurements. Therefore, the deviations between the numerical and experimental results are considered to be within a reasonable range.

5. Conclusions

To meet the airflow distribution requirements of the swirl-straight flow synergistic system, a louver-type pulverized coal distributor is designed in this study. Based on the 2: 1 geometric similarity relationship between the actual equipment and the scaled-down experimental model, cold-state single-phase air modeling experiments and CFD simulations are conducted to investigate the effects of the swirl-side inlet height on airflow distribution, outlet velocity matching, and pressure loss characteristics. The main conclusions are as follows:

1) The designed louver-type pulverized coal distributor enables the redistribution and directional allocation of the primary airflow. After passing through the louver blades, the primary airflow is deflected under the combined effects of blade guidance and local pressure differences. Part of the airflow enters the swirl-side passage, while the remainder flows into the lean-side passage. The research results demonstrate that the louver structure can regulate the primary airflow distribution ratio, providing a flow organization basis for the optimization of the subsequent combustion system.

2) The swirl-side inlet height is a key structural parameter affecting the airflow distribution performance of the louver-type pulverized coal distributor. Variations in the inlet height lead to pronounced changes in the swirl-side outlet velocity, air extraction ratio, and system pressure loss, with the overall response exhibiting an initial increase followed by a decrease. A smaller inlet height enhances local airflow deflection; however, an excessively small flow area intensifies the local contraction effect, increases flow resistance, and limits the effective airflow entering the swirl-side passage. Therefore, reducing the swirl-side inlet height does not necessarily improve distributor performance. Among the six configurations investigated in this study, the 137 mm configuration provided the most favorable balance between outlet velocity matching, swirl-side airflow supply, and overall pressure loss.

3) Considering the swirl-side airflow extraction capability, outlet velocity matching, and system pressure loss characteristics, a swirl-side inlet height of 137 mm is determined as the preferred structural parameter. Under this condition, the swirl-side airflow accounts for 15.17% of the total airflow, the velocity ratio between the swirl-side and lean-side outlets reaches 1.03, and the overall pressure loss coefficient is 0.853. A favorable airflow redistribution effect is achieved.

4) The numerical simulation results reveal pronounced velocity gradients and local flow separation within the louver-type pulverized coal distributor. In the blade region, the airflow is blocked and redirected by the louver blades, producing a deflected flow pattern and low-velocity regions on the leeward sides of the blades. In the curved passage, centrifugal effects lead to further redistribution of the airflow velocity. After passing through the outlet development section, the velocity distributions on both sides gradually become more uniform, indicating that an appropriately designed flow-passage structure can effectively improve outlet airflow uniformity.

5) The numerical method based on the realizable k-ε turbulence model provides satisfactory predictions of the internal flow characteristics of the louver-type pul-

verized coal distributor. The simulated swirl-side airflow fraction of the total airflow is 15.28%, compared with the experimental value of 15.17%, with an absolute deviation of 0.11 percentage points and a relative error of 0.73%. The simulated overall pressure loss coefficient is 0.87, while the experimental value is 0.853, with a relative error of 1.99%. For the selected integral parameters, the relative differences between the numerical and experimental results ranged from 0.73% to 7.10%. The numerical model therefore provides a reasonable representation of the overall airflow redistribution and pressure-loss behavior under the investigated cold-state condition. However, its predictive accuracy for pulverized-coal transport and combustion behavior was not evaluated in the present study.

Funding

This work is supported by the CR Power Theory R & D Program (Grant No. CRP-R & D-LX-2025-031).

Author Contributions

Longzhen Guo: Writing-original draft, Methodology, Formal analysis, Conceptualization. Zhidong Li: Writing-review and editing, Validation, Investigation. Jiahui Zhao: Writing-review and editing, Visualization, Investigation. Defu Xin: Writing-review and editing, Resources, Project administration. Weiyu Wang: Visualization, Investigation, Conceptualization. Hanlin Li: Writing-review and editing, Validation, Investigation. All authors have read and agreed to the published version of the manuscript.

Conflicts of Interest

The authors declare no conflicts of interest regarding the publication of this paper.

References

[1] Li, J., Liu, F., Li, Z., Shao, C. and Liu, X. (2018) Grid-Side Flexibility of Power Systems in Integrating Large-Scale Renewable Generations: A Critical Review on Concepts, Formulations and Solution Approaches. *Renewable and Sustainable Energy Reviews*, **93**, 272-284. https://doi.org/10.1016/j.rser.2018.04.109

[2] Zhang, J. and Zheng, Y. (2020) The Flexibility Pathways for Integrating Renewable Energy into China's Coal Dominated Power System: The Case of Beijing-Tianjin-Hebei Region. *Journal of Cleaner Production*, **245**, Article ID: 118925. https://doi.org/10.1016/j.jclepro.2019.118925

[3] Na, C., Pan, H., Zhu, Y., Yuan, J., Ding, L. and Yu, J. (2019) The Flexible Operation of Coal Power and Its Renewable Integration Potential in China. *Sustainability*, **11**, Article 4424. https://doi.org/10.3390/su11164424

[4] Lannoye, E., Flynn, D. and O'Malley, M. (2012) Evaluation of Power System Flexibility. *IEEE Transactions on Power Systems*, **27**, 922-931. https://doi.org/10.1109/tpwrs.2011.2177280

[5] Wang, D., Liu, D., Wang, C., Zhou, Y., Li, X. and Yang, M. (2022) Flexibility Improvement Method of Coal-Fired Thermal Power Plant Based on the Multi-Scale Utilization of Steam Turbine Energy Storage. *Energy*, **239**, Article ID: 122301.

https://doi.org/10.1016/j.energy.2021.122301

[6] Wang, J., Huo, J., Zhang, S., Teng, Y., Li, L. and Han, T. (2021) Flexibility Transformation Decision-Making Evaluation of Coal-Fired Thermal Power Units Deep Peak Shaving in China. *Sustainability*, **13**, Article 1882. https://doi.org/10.3390/su13041882

[7] Richter, M., Oeljeklaus, G. and Görner, K. (2019) Improving the Load Flexibility of Coal-Fired Power Plants by the Integration of a Thermal Energy Storage. *Applied Energy*, **236**, 607-621. https://doi.org/10.1016/j.apenergy.2018.11.099

[8] Fiebrandt, M., Röder, J. and Wagner, H. (2021) Minimum Loads of Coal-Fired Power Plants and the Potential Suitability for Energy Storage Using the Example of Germany. *International Journal of Energy Research*, **46**, 4975-4993. https://doi.org/10.1002/er.7490

[9] Wang, Q., Chen, Z., Li, L., Zeng, L. and Li, Z. (2020) Achievement in Ultra-Low-Load Combustion Stability for an Anthracite- and Down-Fired Boiler after Applying Novel Swirl Burners: From Laboratory Experiments to Industrial Applications. *Energy*, **192**, Article ID: 116623. https://doi.org/10.1016/j.energy.2019.116623

[10] Chang, J., Wang, X., Zhou, Z., Chen, H. and Niu, Y. (2021) CFD Modeling of Hydrodynamics, Combustion and Nox Emission in a Tangentially Fired Pulverized-Coal Boiler at Low Load Operating Conditions. *Advanced Powder Technology*, **32**, 290-303. https://doi.org/10.1016/j.apt.2020.12.008

[11] Ma, D., Zhang, S., He, X., Ding, X., Li, W. and Liu, P. (2024) Combustion Stability and NO Emission Characteristics of Three Combustion Modes of Pulverized Coal Boilers under Low or Ultra-Low Loads. *Applied Energy*, **353**, Article ID: 121998. https://doi.org/10.1016/j.apenergy.2023.121998

[12] Hong, T., Zuodong, L., Xiaoju, H., Xueqiang, S., Yuqiu, L., Siyuan, W., *et al.* (2024) Experimental Study on Combustion Characteristics of a 40 MW Pulverized Coal Boiler Based on a New Low Nox Burner with Preheating Function. *Energy*, **305**, Article ID: 132319. https://doi.org/10.1016/j.energy.2024.132319

[13] Zhang, H., Shu, Y., Wang, X., Zhou, X., Li, W., Zheng, H., *et al.* (2026) Improving the Flexibility of Coal-Fired Power Plants via a Pre-Gasification Burner with Ultra-Enhanced Flame Stability. *Engineering*, **59**, 229-239. https://doi.org/10.1016/j.eng.2025.04.015

[14] Wang, J., Yang, J., Yang, F. and Cheng, F. (2023) Numerical and Experimental Investigation of the Decoupling Combustion Characteristics of a Burner with Flame Stabilizer. *Energies*, **16**, Article 4474. https://doi.org/10.3390/en16114474

[15] Huang, C., Li, Z., Wang, Y., Lu, Y., Liu, H. and Chen, Z. (2023) Influence of Central Air on Flow and Combustion Characteristics and Low-Load Stabilization Performance of a Babcock Burner. *Processes*, **11**, Article 1916. https://doi.org/10.3390/pr11071916

[16] Ding, H., Ouyang, Z., Su, K. and Zhang, J. (2023) Investigation of Gas-Solid Flow Characteristics in a Novel Internal Fluidized Bed Combustor by Experiment and CPFD Simulation. *Advanced Powder Technology*, **34**, Article ID: 103962. https://doi.org/10.1016/j.apt.2023.103962

[17] Zhou, C., Wang, Y., Jin, Q., Chen, Q. and Zhou, Y. (2019) Mechanism Analysis on the Pulverized Coal Combustion Flame Stability and Nox Emission in a Swirl Burner with Deep Air Staging. *Journal of the Energy Institute*, **92**, 298-310. https://doi.org/10.1016/j.joei.2018.01.006

[18] Liu, T., Wang, Y., Zou, L., Bai, Y., Shen, T., Wei, Y., *et al.* (2024) Numerical Investigation of Stable Combustion at Ultra-Low Load for a 350 MW Wall Tangentially

Fired Pulverized-Coal Boiler: Effect of Burner Adjustments and Methane Co-Firing. *Applied Thermal Engineering*, **246**, Article ID: 122980. https://doi.org/10.1016/j.applthermaleng.2024.122980

[19] Yang, K., Li, Z., Cao, X., Du, T. and Liu, L. (2024) Numerical Simulation Study on the Stable Combustion of a 660 MW Supercritical Unit Boiler at Ultra-Low Load. *Processes*, **12**, Article 2573. https://doi.org/10.3390/pr12112573

[20] Jiang, Y., Lee, B., Oh, D. and Jeon, C. (2021) Optimization of Operating Conditions to Achieve Combustion Stability and Reduce Nox Emission at Half-Load for a 550-MW Tangentially Fired Pulverized Coal Boiler. *Fuel*, **306**, Article ID: 121727. https://doi.org/10.1016/j.fuel.2021.121727

[21] Ju, R., Lu, H., Liu, H., Guo, L. and Hu, H. (2025) Numerical Study on Combustion Characteristics and Nox Emissions in a 600 Mwe Boiler under Half Load: A Study of Single and Blended Coal Types. *Case Studies in Thermal Engineering*, **76**, Article ID: 107365. https://doi.org/10.1016/j.csite.2025.107365

[22] Song, M., Huang, Q., Niu, F. and Li, S. (2020) Recirculating Structures and Combustion Characteristics in a Reverse-Jet Swirl Pulverized Coal Burner. *Fuel*, **270**, Article ID: 117456. https://doi.org/10.1016/j.fuel.2020.117456

[23] Cao, H., Xu, L., Zhang, G., Cui, Y. and Zhang, L. (2026) Research Progress on the Stable Operation of Pulverized Coal-Fired Boilers under Low-Load Conditions. *ACS Omega*, **11**, 12955-12963. https://doi.org/10.1021/acsomega.5c10518

[24] Zhu, S., Zhou, H., Li, Z., Zeng, X., Ouyang, Z., Hui, J., *et al.* (2025) Wide-Load Combustion Characteristics of Lean Coal Tangential Preheating Combustion. *Energy*, **323**, Article ID: 135845. https://doi.org/10.1016/j.energy.2025.135845

[25] Huang, C.Z., Li, Z.Q., Lu, Y., *et al.* (2025) Gas-Solid Flow Characteristics of a Novel Low-Load Combustion-Stabilizing Burner. *Clean Coal Technology*, **31**, 218-228. (In Chinese)

[26] Hamed, A. and Tabakoff, W. (1991) An Investigation in the Variance in Particle Surface Interactions and Their Effects in Gas Turbine. *Journal of Engineering for Gas Turbines and Power-Transactions of the Asme*, **114**, 235-241.

[27] Shih, T., Liou, W.W., Shabbir, A., Yang, Z. and Zhu, J. (1995) A New K-E Eddy Viscosity Model for High Reynolds Number Turbulent Flows. *Computers & Fluids*, **24**, 227-238. https://doi.org/10.1016/0045-7930(94)00032-t

[28] Leong, M., Samuelsen, G. and Holdeman, J. (1998) Optimization of Jet Mixing into a Rich, Reacting Crossflow. 36*th AIAA Aerospace Sciences Meeting and Exhibit*, Reno, 12 January-15 January 1998. https://doi.org/10.2514/6.1998-156

[29] Guan, X.Y. (2011) Study on Gas-Solid Flow Characteristics in a Horizontal Rich-Lean Pulverized Coal Burner. Ph.D. Thesis, Harbin Institute of Technology. (In Chinese)

[30] Martins, L.L., Ribeiro, A.S. and Sousa, J.A. (2019) Calculation of the Flow-Rate Measurement Uncertainty by Means of Pitot Tubes Using the Monte Carlo Method. 18*th International Flow Measurement Conference* 2019, Lisbon, 26-28 June 2019, 1-6.

[31] Joint Committee for Guides in Metrology (2008) Evaluation of Measurement Data-Guide to the Expression of Uncertainty in Measurement. JCGM 100: 2008. 1-116.